

PROGRESS REVIEW • OPEN ACCESS

## The Receptron: a device for the implementation of information processing systems based on complex nanostructured systems

To cite this article: Gianluca Martini *et al* 2022 *Jpn. J. Appl. Phys.* **61** SM0801


View the [article online](#) for updates and enhancements.

You may also like

- [Evolution of magnetism in UCoGe and UCoAl with Ru doping](#)  
Michal Vališka, Petr Opletal, Jiří Pospíšil *et al.*
- [Hydrogen induced changes in the crystal structure and magnetic properties of UCoGe](#)  
A M Adamska, L Havela and S Daniš
- [Nonlinear Magnetohydrodynamics](#)  
V. Shafranov



# The Receptor: a device for the implementation of information processing systems based on complex nanostructured systems

Gianluca Martini , Matteo Mirigliano, Bruno Paroli, and Paolo Milani\* 

CIMAINA and Dipartimento di Fisica "A. Pontremoli", Università degli Studi di Milano Via Celoria 16, I-20133 Milano, Italy

\*E-mail: [paolo.milani@mi.infn.it](mailto:paolo.milani@mi.infn.it)

Received January 10, 2022; revised March 7, 2022; accepted April 10, 2022; published online June 14, 2022

Unconventional Computing (UComp) identifies several data processing paradigms focused on exploiting emergent complexity and collective phenomena from various classes of physical substrates. Among UComp platforms, neuromorphic artificial systems aim at the reproduction of the human brain functions in terms of classification and pattern recognition capabilities, overcoming the limitations of traditional digital computers and closing the gap with the energetic efficiency of biological systems. Here we present a model, the receptor, and its physical implementation via a neuromorphic system which opens the way for the exploitation of complex networks of reconfigurable elements. Recently we have reported that nanostructured Au films, fabricated from gold clusters produced in the gas phase, have non-linear and non-local electric conduction properties caused by the extremely high density of grain boundaries and the resulting complex arrangement of nanojunctions. Exploiting these non-linear and non-local properties we produced and tested a device, based on a generalization of the perceptron, named receptor, that can receive inputs from different electrode configurations and generate a complete set of Boolean functions of  $n$  variables for classification tasks. The receptor allows also the classification of non-linearly separable functions without previous training of the device. Spatial correlations and the re-organization of the nanojunctions of the cluster-assembled film upon the application of suitable electrical stimuli are the enabling features for the efficient exploration of an extremely large number of weights configurations and hence the capability of the receptor to perform complex tasks.

© 2022 The Japan Society of Applied Physics

## 1. Introduction

The theoretical and practical limitations of the standard computational hardware platforms are urging the development of new substrates, new software and even new paradigms for data processing.<sup>1-3</sup> To date, the wide majority of computers adopt the Turing paradigm<sup>4</sup> in which the act of calculation (regardless of whether a human or a machine performs it) is based on both internal and external states, together with the transition rules between these ones.<sup>4</sup> An infinite tape containing the inputs (external states) is supplied to the computer: this provides a sort of memory and a natural means of communication with a user.<sup>4</sup> This approach offers the possibility of accurately describing what a Turing machine can or cannot calculate, having an immediate translation into a physical device: it must be characterized by a clear distinction between a memory unit and a data processing one, and by frequent exchange of information between these two, costing time and significant energy.<sup>5</sup>

The energy consumption intrinsic to this scheme hampers the capability of matching the performances of mammalian brains with the same efficiency: our encephalon can work with an energy budget of around 20 Watts, whereas its simulation with a computer with the same processing and storage capabilities would require several terawatts of power.<sup>6</sup> Human brain can efficiently retrieve information from limited or noisy inputs with extremely low power consumption and significantly outperform digital computers in tasks such as image recognition, linguistic comprehension, abstract reasoning and classification. Brain architecture is characterized by a complex network of a large number of neurons with an even bigger number of connections between them. The non-linear electrical conduction properties of neurons,<sup>7</sup> typified by voltage spikes,<sup>7,8</sup> and the plastic response of their connections (synapses), allow a massive

parallel elaboration, memory storage functions, self-learning, and adaptive capabilities.<sup>7,9-11</sup>

The synapses which bridge neighboring neurons allow the transmission of the electrical spikes produced by a neuron to the post-synaptic one(s).<sup>7</sup> The strength of this connection, i.e. the synaptic weight, together with the number of spiking pre-synaptic neurons, determines the probability that the post-synaptic will fire too.<sup>7</sup> One of the most important features of synapses is their plasticity, which gives them the possibility of changing the synaptic weight: the latter evolve according to a mixture of the exact timing and frequency with which the two neighboring neurons spike.<sup>7</sup>

Major efforts to reproduce the brain capabilities in terms of classification and pattern recognition have been focused on the development of the so-called "neuromorphic systems" overcoming the limitations of traditional digital computers and closing the gap with the efficiency of biological systems.<sup>3,11,12</sup> A predominant position is occupied by artificial neural networks (ANNs) thanks to their ability to perform tasks such as pattern recognition with high efficiency and relatively low energetic costs.<sup>13,14</sup> The simplest ANN unit is the *perceptron*, a single node ANN, originally proposed by Rosenblatt,<sup>15</sup> and designed specifically to implement an adjustable logic operation through the calibration of "synaptic weights":<sup>14,16-18</sup> the perceptron binary output is the result of a thresholding process performed on the weighted sum of the inputs.<sup>18</sup>

A single perceptron can be used as a boolean classifier, but due to its working principle it can only generate linearly separable Boolean functions (see the XOR problem for the single layer perceptron in<sup>18</sup>); more complex mappings can be achieved via a neural network, an arrangement of two or more layers of perceptrons (multilayer perceptron): if the resulting architecture contains a sufficient number of layers, it is guaranteed to approximate any desired function.<sup>16,19</sup> The



price to pay for the increased number of layers is the rise in training complexity and, correspondingly, in computational (and energetic) costs.<sup>20,21)</sup>

Memristors have been proposed for the physical realization of the perceptron synaptic weights for ANN hardware.<sup>14,22)</sup> The use of memristors allows the physical encoding of these weights: the inputs superposition, i.e. computation, and their memory, that is the physical state of the system, are realized in the same hardware with substantial power reduction compared to standard digital components.<sup>14,23)</sup>

A radically different approach, named “unconventional computing” (UCOMP) is based on the use of hardware and physical architectures relying on emergent complexity and collective phenomena originating from various classes of physical substrates.<sup>1,2,24–28)</sup> UCOMP appears particularly interesting for the classification of complex features: non-linear projection into a high-dimensional space can make data linearly separable, providing classification solutions that are computationally very expensive with digital computers.<sup>28,29)</sup> Examples of UCOMP approaches include optical computing,<sup>30)</sup> molecular computing,<sup>31)</sup> chemical computing<sup>32)</sup> and computing in materia.<sup>33,34)</sup>

UCOMP devices can be fabricated from networks consisting of a large number of non-linear nanoscale junctions resulting from the self-assembling of nanoparticles or nanowires<sup>35–37)</sup> and characterized by spatiotemporal correlation in the electrical activity, in close analogy with the brain structure.<sup>26,35,38)</sup> This behaviour emerges from the presence of high density of non-linear and recurrent junctions formed at the nanoscale during the fabrication process,<sup>35,37,38)</sup> in particular nanowire networks have shown long-term connectivity retention,<sup>39)</sup> hierarchical collective dynamics,<sup>37)</sup> and heterosynaptic plasticity.<sup>36)</sup>

Recently we have shown that nanostructured Au films fabricated from the assembling of gold clusters produced in the gas phase have a complex resistive switching behaviour.<sup>40–42)</sup> Their electric conduction properties are deeply affected by the extremely high density of grain boundaries resulting in a complex network of nanojunctions.<sup>40–42)</sup> Correlations emerge among the electrical activity of different regions of the film under the application of an external electrical stimulus higher than a suitable threshold. The degree of correlation can be varied controlling the film geometry and the electrode configuration used as input and output.<sup>43)</sup>

By interconnecting a generic pattern of electrodes with a cluster-assembled Au film, we demonstrated the fabrication of a device, called receptron, that can perform the binary classification of input signals, following a thresholding process, to generate a set of Boolean functions.<sup>43)</sup> The model of the receptron is a generalization of that of the perceptron: in the latter case, the weights associated with each input are independent and can be individually adjusted to give the desired output. In the case of a receptron, the weights are not univocally related to a single input since the hardware consists in a network of highly interconnected non-linear junctions regulating their connectivity and the topology of conducting pathways depending on the input stimuli.<sup>43)</sup>

The relationship between a perceptron and a receptron can be qualitatively shown by using the analogy represented in Fig. 1 where a series of communicating water fountains is

depicted. In Fig. 1(a) the water fountains generate two independent water fluxes representing a 2-input Perceptron. Boolean inputs are represented by the water taps, “0” for closed tap and “1” for opened: the water flux can be regulated through valves and independently controlled in order to obtain, after the final thresholding, the desired digital output.

A 2-input receptron [Fig. 1(b)] operates a weighting process where both inputs can influence the two outputs (the two water paths are interconnected): in this case, the weights are not independent of one another, unlike the perceptron. Complex interactions between signals coming from the inputs (represented in the figure as the water basin connected to the two outputs) make the outputs correlated. The outputs can be changed by adjusting the weights through valves that can regulate water flux. At odd with the perceptron, the receptron cannot associate a separate weight to each input, due to the complex interactions between the different water paths: weights are not uniquely defined for a set of inputs. This fact has several important consequences such as the capability of a single receptron (i.e. a single device and not a network of devices) of implementing non-linearly separable functions, as we demonstrated in.<sup>43)</sup>

The non-linear and non-local behaviour typical of nano-granular Au films are at the basis of the receptron behaviour: the extremely large number of conduction states that characterize the network of nanojunctions in a cluster-assembled film allows the classification of non-linearly separable functions without previous training of the device.<sup>43)</sup> This is quite surprising and, at a first glance, at odds with one of the basic characters of ANN and UCOMP: the need for training of the network in order to achieve the desired performance. Here we will concentrate on the fact that a receptron can be used without any *a priori* knowledge of the correct weights that need to be implemented. The role of spatial correlations and of the re-organization of the nanojunctions of the cluster-assembled film upon the application of suitable electrical stimuli will be highlighted as enabling the efficient exploration of an extremely large number of weights configurations.

## 2. Materials and methods

Multi-electrode devices based on nanostructured Au films were fabricated by a Supersonic Cluster Beam Deposition apparatus<sup>44)</sup> equipped with a Pulsed Microplasma Cluster Source (PMCS) that allows the production of neutral clusters in gas phase as described in detail in Refs. 44–46. Briefly, the PMCS principle of operation consists in the ablation of a gold target by a plasma ignited during the injection of a high-pressure pulse of argon. The species resulting from the target ablation condense through collision with the Argon gas forming Au clusters, then the cluster-gas mixture is expanded through a nozzle resulting in a supersonic seeded beam.<sup>46)</sup> The cluster beam is focused by an aerodynamic lens system<sup>46)</sup> and directed on silicon substrates where a silicon oxide layer has been previously formed by thermal annealing.<sup>42)</sup> The substrates are equipped with gold electrodes deposited by thermal evaporation.

Figure 2(a) shows the scheme of a multi-electrode device: 6 electrodes, 3 on the left side and 3 on the right side, are connected through the cluster-assembled film. The shape of the cluster film, a square 5 mm × 5 mm, is achieved through a masking process as shown in Fig. 2(a).

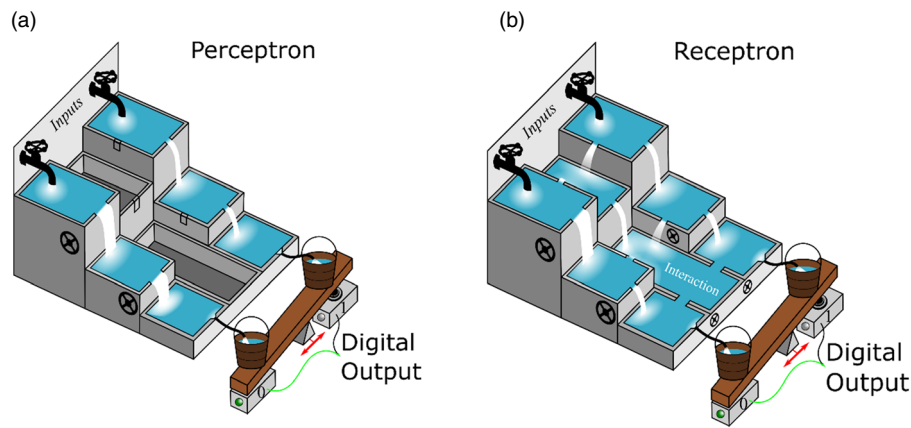


**Fig. 1.** (Color online) Comparison between the abstract models of the perceptron (a) and the receptron (b), the main distinction being the mutual interaction which characterizes the latter. The output is obtained as the difference between the two fluxes collected at the end of the staircase-fountain. Changing the water flux in any case allows us to regulate the output as a function of the inputs given: in most physical realization this is a result of thermodynamic evolution of the system. The perceptron, which lacks any “interaction tank,” is constrained to satisfy linear superposition: the output when both inputs are at full capacity is determined as the sum of the outputs obtained when each input is separately active ( $f(11) = f(10) + f(01)$ ). Therefore, the receptron model has more degrees of freedom and is not limited to linearly separable functions.

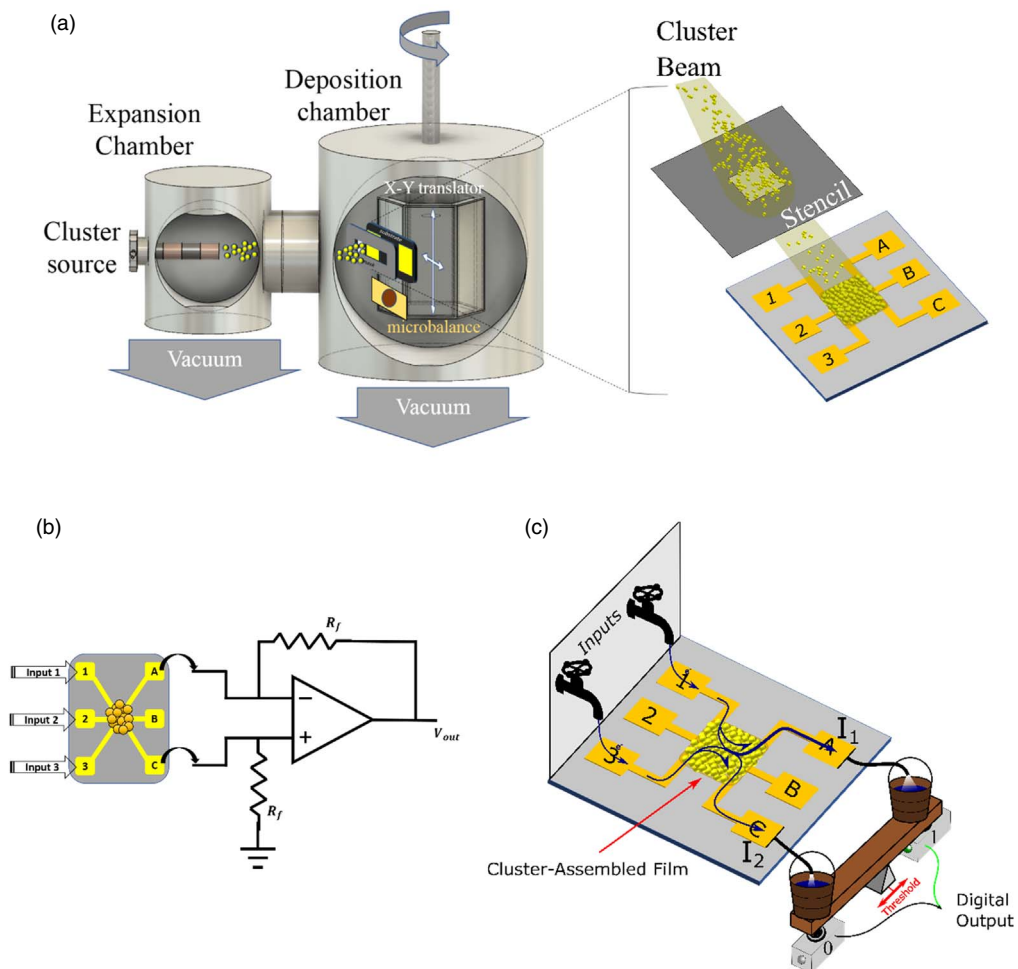


**Fig. 2.** (Color online) (a) Schematic representation (not to scale) of the SCBD apparatus. (b) Circuitual scheme of the receptron: a multi-electrode film is used to elaborate input signals coming from three electrodes on the left (1, 2, 3). Voltage output is proportional to the difference of currents flowing through two right electrodes (A and C), computed by an op-amp used in differential configuration. Note that both the Input and op-amp connections may be rearranged in any desired way to obtain a different overall behaviour from the very same substrate. In what follows, a measure between electrodes 1 and A will be referred to as electrode-couple 1-A (c) schematic view of the working principle of a receptron implemented through a cluster-assembled film. The complex and plastic nanostructured gold film allows us to rearrange the current flow, hence the output, in full analogy with the model of interconnected water fountains.

In order to analyze the device performances, we employed all the available electrodes either as input or as output: the pins on one side were used to apply potential differences while the ones on the opposite were connected with the op amp to obtain the electrical output. Note that this decision is arbitrary, since such a system poses no *a priori* limit on the role of different pins: one can take advantage of combinatorics in using the device, since a simple rewiring will change the output mapping.

High potential differences ( $\Delta V > 5\text{V}$  for samples of  $1\text{cm}^2$ ) applied on the film trigger the reorganization of nanoscale junctions, which in turn produces a macroscopic change of resistance. This defines a threshold voltage  $V_T \sim 1\text{V}$  that distinguishes the so-called Read operations from the Write ones: the first consist of sub-threshold stimuli used to detect the current state of the receptor, while the latter consist of higher voltage applications (up to  $+35\text{V}$ ) meant to induce rearrangements inside the film. The standard protocol used to investigate these structural changes consists of Read, Write, Read series of operations. The first Read operation detects the initial condition of the film, which is modified by the high current flow due to the Write phase: the successive Read one will then determine what is the final state of the system. The resistive switching phenomenon directly impacts the conduction properties of several regions of the film, which in turn result in a different current flow and a new receptor output voltage. For this reason, the “Read, Write, Read” protocol has been used for both electrical- and device performance-characterization.

For both types of measurements, we used a Keysight E5270 electrometer, remotely controlled via ad hoc LabView programs, as a (pulsed/constant) voltage source and for the current measures. An Arduino was used to toggle the relays needed to select which electrodes of the film were used.

During characterization phase, a train of 10 voltage pulses higher than  $5\text{V}$ , width in the range  $100\text{--}500\text{ms}$  (writing voltage) is applied to one electrode configuration, consisting of one set of input electrodes and one set of output electrodes. This writing phase triggers local rearrangement of nanoscale contacts between grains [see inset in Fig. 2(a)] and the consequent reorganization of paths of minimum resistance followed by electron current. A reading phase (20 voltage pulses, height  $1\text{V}$ , width  $70\text{ms}$ ) is then applied in order to probe the resistance of each electrode couple, consisting of one input electrode and one output electrode: all electrode couples are characterized serially after each writing step.

Figure 2(b) shows the circuitual scheme of a perceptron, where a multi-electrode cluster-assembled film (CAF) is used to implement a physical relation of the model presented above. The electrodes on the left (1, 2 and 3) are used as input electrode, where current is injected. Electrodes on the right (A, B and C) are used as output electrodes. The details of the implementation can be found elsewhere.<sup>43)</sup>

### 3. Results and discussion

The cluster-assembled Au film nanostructure, rich in grain boundaries and defects, produces a markedly non-Ohmic characteristic for all current paths inside the film and a hysteresis, especially visible in the positive branch of  $I\text{--}V$  curves, as shown in Fig. 3 (see the rightmost plot). The application of a potential difference results in a non-linear

conduction regime with each electrode-couple bridged by a different resistance. Paths sharing a common electrode have a similar current-voltage characteristic. Asymmetries with respect to the polarity of the applied voltage appear in the  $I\text{--}V$  curves, probably due to local structural characteristics of the device.

These peculiar electrical properties are largely determined by the granular structure at different length scales that characterizes these systems: although the elemental building blocks can be considered metallic, their assembly does not result in an overall ohmic conductor.<sup>40–42)</sup>

Electronic carrier conduction in nanostructured systems can be considered to be based on space charge limited conduction mechanisms and coulomb blockade<sup>47,48)</sup> with very strong geometrical constraints.<sup>49–51)</sup> The presence of an extremely high density of grain boundaries and crystalline orientation mismatches represents a barrier for electric charges, deeply affecting the electrical conduction:<sup>52–55)</sup> a distribution of different local resistances is formed over the whole cluster-assembled film.<sup>56,57)</sup>

What is more, these defects can be plastically modified through breaking and reconstruction of nanoscale junctions between metallic grains due to electromigration and joule heating.<sup>56)</sup> As a result, the energy dissipation coming from current flow can give rise to rearrangement phenomena near the grain boundaries: a new distribution of conductance values inside the film is established and a new macroscopic resistance is reached, as indicated by the hysteresis in  $I\text{--}V$  curves of Fig. 3. It is thus clear that the different macroscopic resistance values characterizing every electrode-couple depend on the sample history, i.e. which and (most importantly) where electrical stimuli are applied.<sup>43)</sup>

We can follow this dynamical evolution  $R(t)$  thanks to the Read, Write, Read protocol, aimed at maximizing the induced modifications: this is presented in Fig. 4 for two paths inside the film. The nanoscale rearrangements result in sudden changes of global Resistance: a resistive switching behaviour, triggered by write voltages, is observed.<sup>40,42)</sup> After every Write voltage application (marked by the vertical grey lines), the film exhibits a new resistive value.

Figure 4 also shows that different regions of the film display a distinct evolution in time in response to the very same stimuli: see how different the behaviour of 1-A and 2-B is. In addition, we highlight the presence of mutual interactions between current paths: these detect write phases even if performed on different regions of the film (see the green arrows). In other words, the network responds in a non-local, collective way to high voltage stimuli. Two main phenomena are responsible for such a cooperative behaviour: on one hand, the potential difference is fixed from outside, thus the modification of part of the network must be compensated by the rest of the system. On the other, the electrical current flow causes joule heating and electromigration, inducing rearrangement phenomena and grain boundary modifications in vast portions of the network: these can themselves trigger more resistive switches.<sup>40–42)</sup>

Such non-local effects manifest themselves into extensive spatiotemporal correlations inside the film, an example of which is shown in Fig. 5. Comparing the evolution of different regions of the film (that is, electrode couples), we notice that some tend to respond in the same way to the



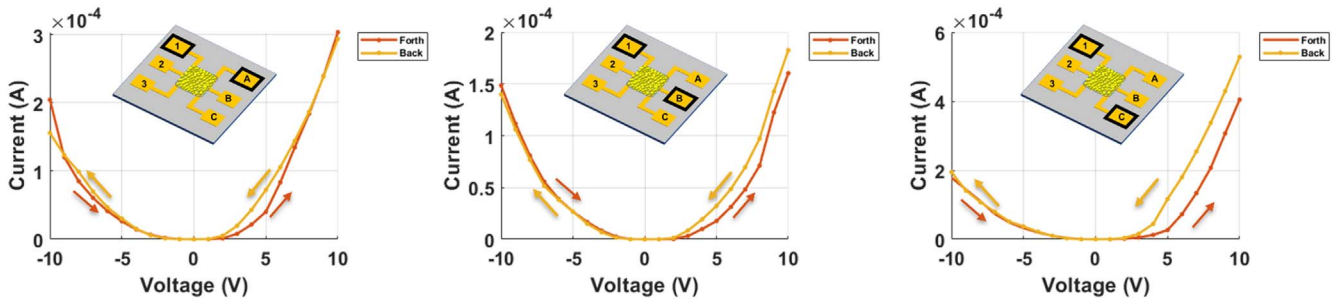


**Fig. 3.** (Color online)  $I$ - $V$  Curves ( $-10\text{V}:1:10\text{ V}$ ) obtained from a multi-electrode CAF sample: the small inset on the right corner of each plot indicates the electrodes that were used to apply the  $\Delta V$  and obtain the curve. The non-Ohmic behaviour is apparent as well as an asymmetry between the positive and negative branch. Note the hysteresis between forward and backward curves, particularly with  $\Delta V > 0$ .

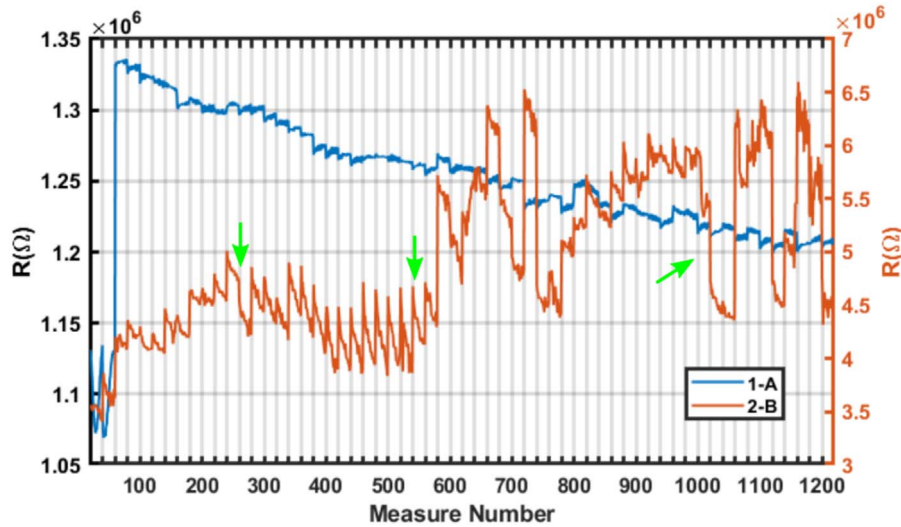


**Fig. 4.** (Color online) Evolution of resistance over time of two different electrode configurations (orange curve electrodes 2-B and blue curve electrode 1-A): note that the data are referred to two different vertical axes (1-A to the left and 2-B to the right one). Grey vertical lines are placed in correspondence of writing phases: after each of them, all couples were sequentially read to measure their resistance. Writing phases consisted of 5 positive and negative voltage pulses selected between 5 V and 35 V lasting 0. Read pulses were successively performed on all electrode-couples and consisted of 20 pulses of 1 V, each with a duration of 50 ms. We observe several spikes occurring right after a writing stimulus applied there or on a nearby region. Some of the biggest switches on 2-B (marked by the green arrows) were triggered by electrical stimulations that did not involve either of these two electrodes directly.

stimulus while others do not: this translates in a higher or lower correlation between the two  $R(t)$  graphs. The overall pattern is far from being trivial: e.g. the time evolution couples 1-A and 3-A, but not 1-A and 2-A which share a much larger portion of the film. The complexity of the system is signalled by the co-existence of both high and very low ( $|\rho| < 0.3$ ) correlation: each extremum of this spectrum would result in a much simpler network behaviour. Similar complex behaviour has been reported for Ag nanowire networks,<sup>58</sup> and highlighted by the use of a  $9 \times 9$  associative matrix. By increasing the number of our electrodes, we do expect to achieve more detailed information about the extent of spatially interconnected regions.

Summarizing, a multi-electrode gold CAF can be described as a collection of the resistive states of the different regions of the film, which are themselves a function of time or, more appropriately, the number and location of *write* pulses that have previously been applied. This is depicted in Fig. 6 which shows a representation of the dynamics of system states following the application of write voltage pulse trains: note how some of the regions evolve in a closely related, that is *correlated*, way.

These electrical features implement the different aspects of the receptor (Fig. 2). Write phases act as the valves, altering

the “water” flow and the analog output, while the current redistribution as well as joule heating are responsible for the physical interaction between the outputs (the “interaction tank”). Thanks to the nanoscopic rearrangements, we have thus obtained a reconfigurable analog input-output mapper.

An example of its functioning is shown in Fig. 7, where some analog outputs obtained with 200 write steps are plotted: the output voltage explores a wide range of values for every input (note that the “noisy” appearance of such an evolution is due to the write phases, not to any instability of the system:<sup>43</sup>) we have shown that the read phase uncertainty is much less than the resistive switch induced by excitatory stimuli (in symbols,  $\Delta R_{Write} \gg \sigma_{Read}$ ).

This promising plethora of behaviours, however, cannot be directly and accurately controlled: because of the extremely high number of junctions involved and the metastable configurations of the system, it is very difficult (if not impossible) to predict the system trajectory in the configuration space. In other words, the  $R(t)$  dynamics will always be somewhat random and unpredictable (see also Fig. 4). This stochasticity will obviously manifest itself also in the output of the device, as shown in Fig. 2, which is just an elementary combination of several current flows. Therefore, one could not exploit this device à la Turing, that is in a pre-

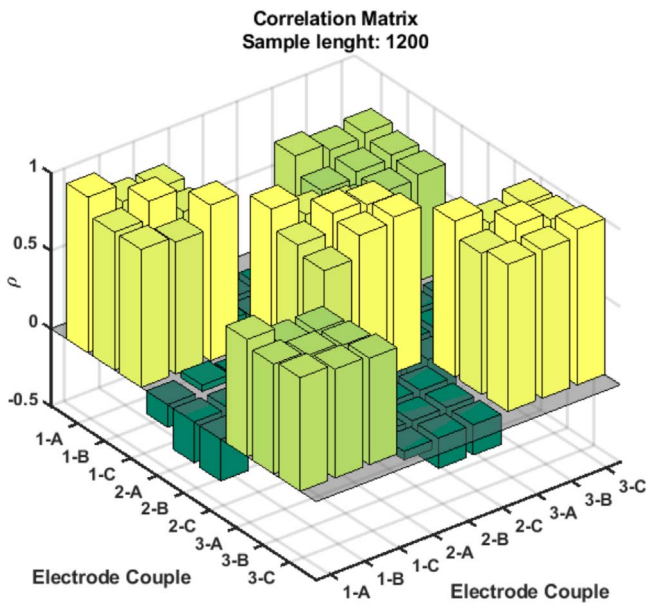


**Fig. 5.** (Color online) Correlation matrix: the  $(i, j)$ th column's height and colour display the value of Pearson's  $\rho(R_i, R_j)$  coefficient for the resistance reading between  $i$ th electrode couples and the  $j$ th one, indicating how close their two evolutions are. Writing steps consisted of 5 pulses of 0.5 s each with a voltage magnitude randomly selected between 5 V and 35 V (both positive and negative), while reading steps comprised 20 0.05 s pulses of 1 V. For example, the leftmost yellow column indicates that  $\rho(1 - A, 1 - A) = 1$ . Similar correlation values are grouped with the same colour to help understanding how collections of similar behaviours are found.

programmed and deterministic way: we can instead use this complex system to rapidly explore a variety of input-output applications until the right one is reached.

This random search approach is intrinsically different from the *training* performed for classical ANNs: while classical neural networks require fine tuning of weights of each single device according to some gradient descent technique,<sup>59)</sup> our approach relies only on a random change of the interconnected weights. The non-local effects in the conduction mechanism in a nanojunction system results in a correlated

behaviour, characterized by the simultaneous changes in the resistance of different regions of the film.<sup>43,58)</sup> The generated voltage outputs are not statistically independent and the device explores only a subset of the whole set of the possible outputs, by using an output thresholding strategy, we can reduce the dimensions of the subset thus improving the efficiency of the random search approach.<sup>43)</sup>

In particular, we have boosted the efficacy of this random search protocol with a digitalization of the device. The main idea is to exploit a thresholding process coupled with the non-local spatio temporal correlations of CAFs, to influence the output evolution with little control on the underlying, complex, system dynamics. The thresholding process converts the analog output of the device into a digital value, i.e. “above” or “below” a certain value (or “inside” versus “outside” a certain interval for a band thresholding). Just as for any digital system, this has the immediate advantage of suppressing the effect of electrical noise in the device functioning, but also greatly simplifies its integration with conventional electronics.

We therefore obtain a Boolean function generator which randomly changes its truth table. The device plasticity originating from write phases allows to rapidly explore a wide variety of outputs: it was recently shown<sup>43)</sup> that a single receptor is capable, after just 80 writing steps, to produce a third of all the 3-input Boolean functions. The main difference with respect to the analog generation process is that now we can tune the statistics through the threshold. Fixing a particular threshold, the device produces different boolean output functions as the analog values fluctuate above and below the chosen grey plane (see the three b/w graphs in the centre of Fig. 7). Calibration of the threshold with respect to the average output value will shift the frequency distribution of black and white pixels, as presented in the rightmost column of Fig. 7.

There is, however, an additional degree of freedom linked to the thresholding process which turns out to be particularly useful as a further tool to adjust the kind of the output function produced. As can be seen from the left and central

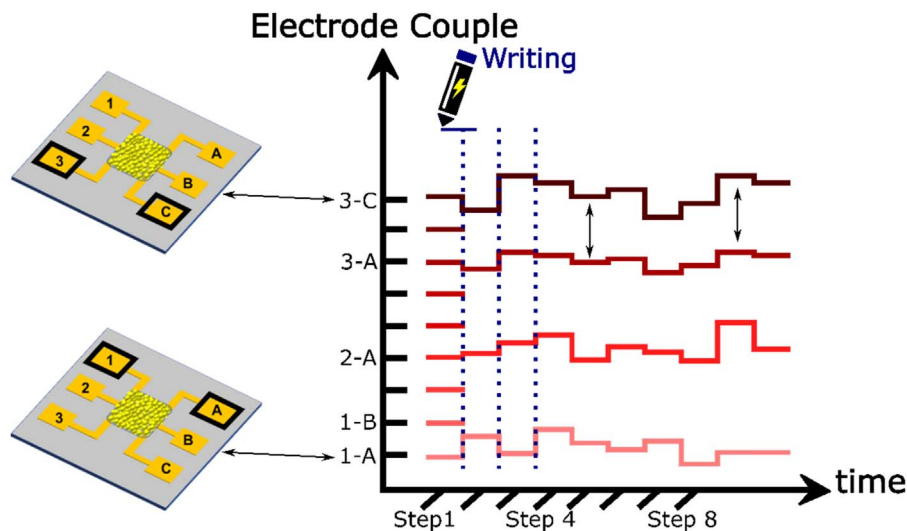


**Fig. 6.** (Color online) A graphical representation of the evolution of different current paths (4 are shown) at different time steps (placed on  $x$ -axis) corresponding to different electrode configurations (placed on  $y$ -axis). Electrical resistance of each electrode couple represents a CAF state at each step, i.e. before a new writing process. The type of writing steps described in the Materials and Methods section cause different reading outputs as a result. Note how non-local correlations can emerge between different regions of the film: in this case 3-C and 3-A show a fully analogous response, although on different scales.

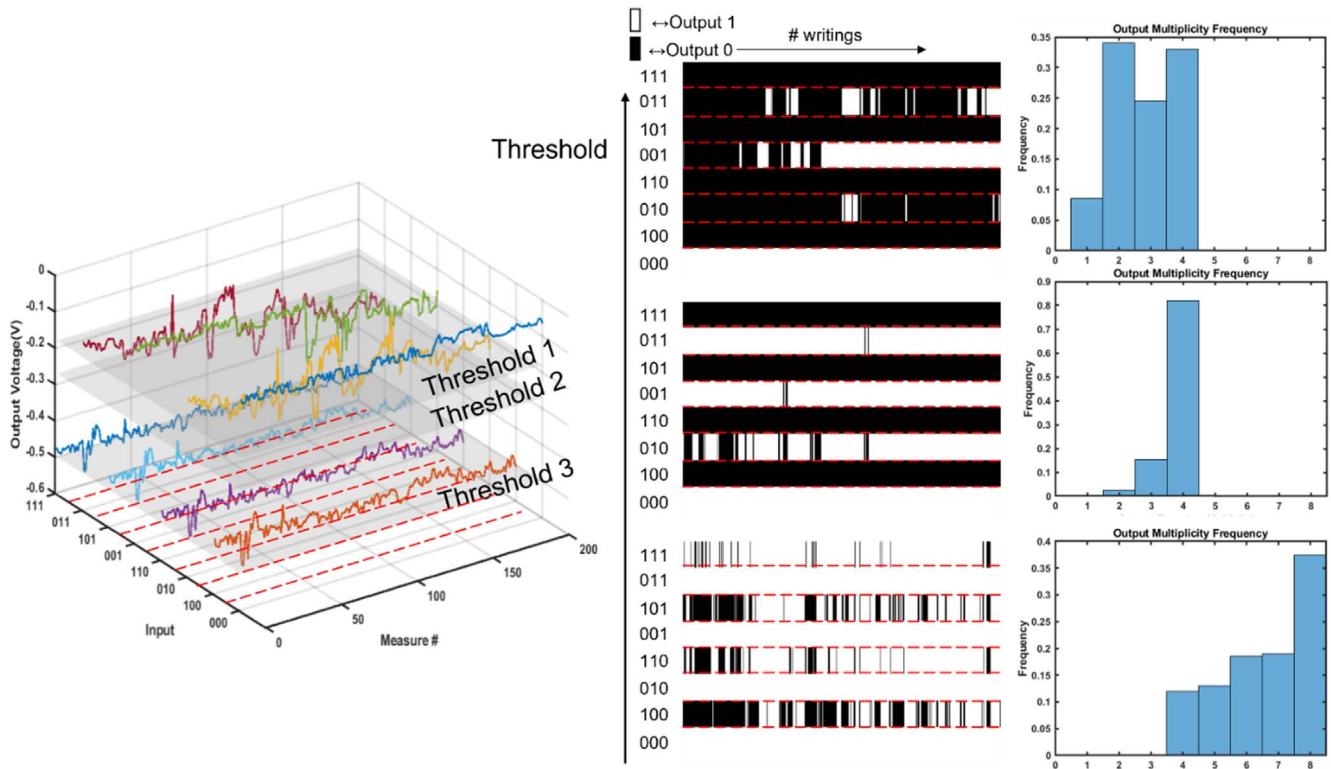


**Fig. 7.** (Color online) Effect of thresholding on the analog output data for different inputs. On the left the (analog) outputs are represented as a function of time and logical input (100, 010, 001 etc.); in the central column the digital outputs obtained with three different thresholds (grey planes in the left plot) are shown (white = above threshold, black = below). The output distributions can be regulated through the choice of the threshold: for example, a higher one will favour black outputs. This is quantitatively represented by the histograms on the rightmost column: they show the multiplicity (i.e. the number of “1” in the output function) distribution of the outputs obtained with the three thresholds shown. As we move to lower values of the latter parameter, the distribution shifts to higher number of multiplicities: more ones/white spots are present.

parts of Fig. 7, some outputs appear to be more similar both in their mean value and in their overall dynamical evolution (see for example the ones corresponding to inputs “111” and “101”). This is a consequence of the correlations between different conductive routes inside the CAF already described in Fig. 5.

Far from being a mere inconvenience, correlations can be used to change the characteristics of the digital function physically implemented by the substrate: they allow to restrict the Boolean function to respect some constraint. If, for example, the output corresponding to input 100 and 010 are highly correlated (but independent from all the others), they will fluctuate above and below the threshold simultaneously. Therefore, the two outputs are either (0, 0) or (1, 1) but not (1, 0) or (0, 1). This introduces bonds between *a priori* fully independent variables (the  $2^n$  output values corresponding to the  $n$  inputs): such a constraint helps to focus the random search on the type of output functions which are of the greatest interest rather than to equally sample all the possible digital outputs. In other words, exploiting the joint effect of correlations and thresholding, we can “fix the dices” of our random search for the desired function, in order to increase the probability of producing the “right” output.

The combined effect of correlations and thresholding is presented in Fig. 8 where both different thresholds and correlations have been explored such as to give a perspective view. Moving along a column we see the same effect of Fig. 7, i.e. the higher the threshold, the more the distribution

will shift to blacks. Moving along the rows, instead, displays the effect of different kinds of correlations between the outputs i.e. how correlations provide one additional parameter which can be used to further specialize our exploration of output space.

Note how the different scenarios displayed in the three columns do not require the fabrication of different samples: the correlations between outputs depend on the sample characteristics but also on the op-amp-film connections. As an example, the two radically different output correlations shown in the first and last columns of Fig. 8 were obtained from the very same film just by changing the wirings of the circuit [see Fig. 2(b)]. Therefore, thanks to the non-trivial correlation pattern found in a complex system (like the experimental one from Fig. 5), we can achieve radically different behaviour just by using different electrodes as output pins. This workaround allows to fully exploit the self-organization of the network, rather than engineering the device to match prespecified parameters: the network can be used as it is, even without a quantitative knowledge of how it works.

#### 4. Conclusions

Nanogranular Au films fabricated from the assembling of gold clusters by supersonic cluster beam deposition are composed by a large number of non-linear nanoscale junctions and show non-linear conduction properties characterized by spatiotemporal correlation in their electrical activity. Starting from these systems we fabricated a device called



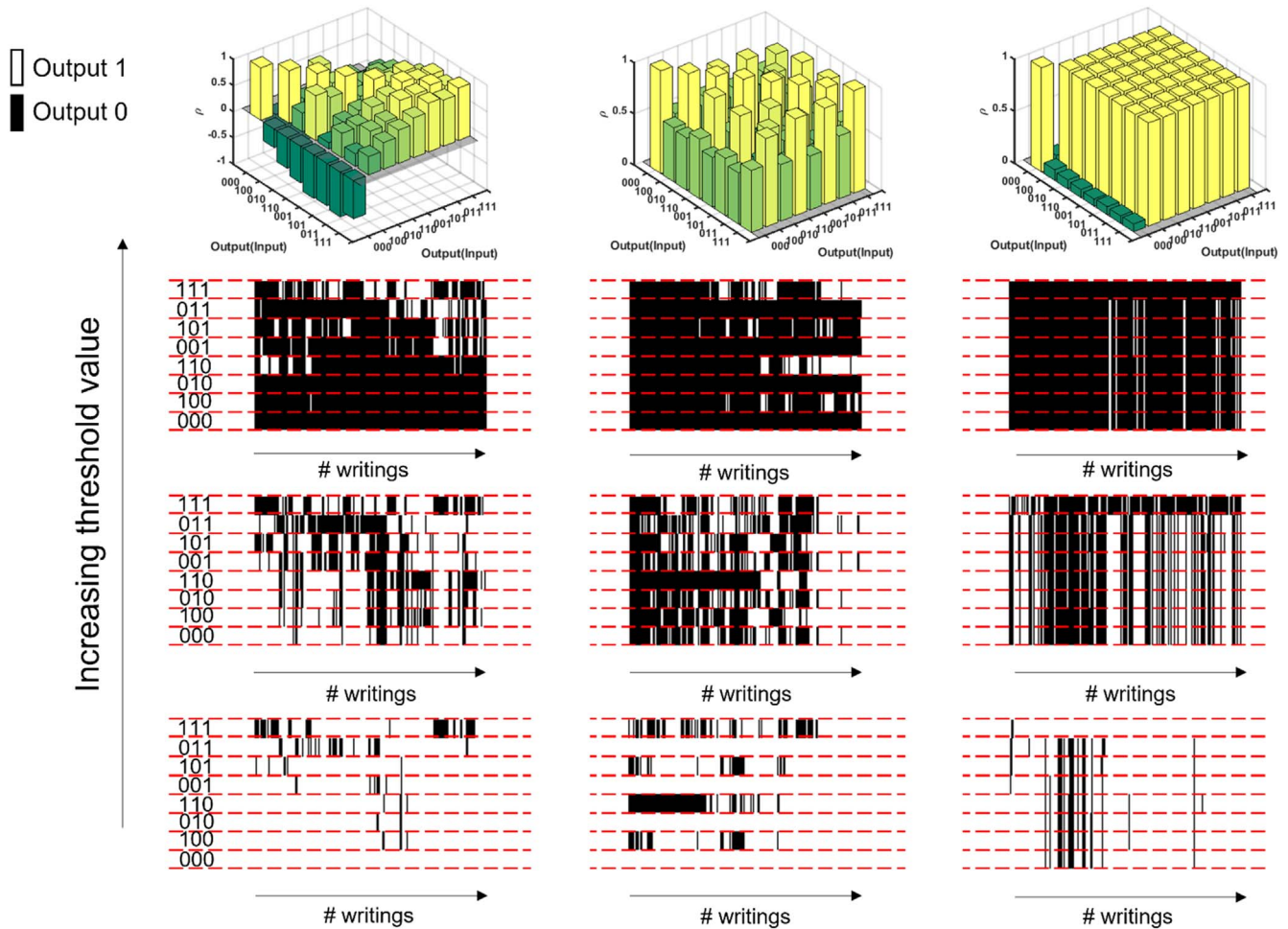


**Fig. 8.** (Color online) Digital Outputs after thresholding as a function of input combination and time (# of writing steps performed) for three scenarios characterized by different correlations: the correlation matrix between the (digital) outputs corresponding to the various inputs are shown above. (Note that this matrix is a result of the correlations between current paths inside the film (like the ones shown in Fig. 5) but can look very differently, depending on how the film/op-amp connections are established). Each row of b/w plots is obtained with a different choice of threshold, producing an effect already described in Fig. 7: the higher the threshold, the more black dots (Output = 0) are to be found and vice versa. As we increase correlations, the outputs tend to be more similar and thus only a particular subset of the whole Boolean function space is explored: this is particularly evident in the second row, third column plot (see how correlated most outputs are), where typically only functions of the type  $\bar{x}xxxxx$  (where  $x = 0, 1$  and  $\bar{x}$  indicates the negation of the Boolean variable) are found, while in the right bottom corner, outputs like  $\bar{x}xxxxx$  and  $xxxxxxx$  are equally likely.

receptor, as a generalization of the perceptron, that can receive inputs from different electrode configurations and generate a complete set of Boolean functions of  $n$  variables for classification tasks. Correlations emerge among the electrical activity of different regions of the film under the application of an external electrical stimulus higher than a suitable threshold. The degree of correlation can be varied controlling the film geometry and the electrode configuration used as input and output. The receptor can perform the binary classification of input signals, following a thresholding process, to generate a set of Boolean functions.

A random search protocol is effective to obtain a binary classification of the input thanks to the exploitation of the extremely large number of conduction states typical of a complex network of nanojunctions. We also gave a quantitative estimation of the efficiency in using the same device as Boolean function generator. The structural properties of cluster-assembled films make the device reliable and fault tolerant against possible fabrication drifts.

Our results open new perspectives for the use of cluster-assembled metallic films for the fabrication of reconfigurable classification devices and for the use of the intrinsic

properties of complex nanojunction networks to implement information processing systems. In particular, the simple structure of the receptor and the use of SCBD for fabrication favour the integration of these devices on microfabricated platforms and polymeric substrates<sup>60</sup> for wearable systems exploiting edge computing via unconventional data processing.

**ORCID iDs**

Gianluca Martini <https://orcid.org/0000-0003-3993-5711>  
 Paolo Milani <https://orcid.org/0000-0002-8799-3070>

- 1) H Jaeger, *Neuromorphic Comput. Eng.* **1**, 012002 (2021).
- 2) C. Teuscher, *Front. Robot. AI* **1**, 1 (2014).
- 3) E. Chicca, F. Stefanini, C. Bartolozzi, and G. Indiveri, *Proc. IEEE* **102**, 1367 (2014).
- 4) J. E. Savage, *Models of Computations* (Reading, MA), (Addison-Wesley, 1998).
- 5) J. Backus and Commun, (New York), (ACM) **21**, 613 (1978).
- 6) N. Jones, *Nature* **561**, 163 (2018).
- 7) E. R. Kandel, J. H. Schwartz, and T. M. Jessell, *Principles of Neural Science* (New York), (McGraw-Hill, 2000) 4th ed.
- 8) E. M. Izhikevich, *IEEE Trans. Neural Networks* **14**, 1569 (2003).

- 9) G. Tononi, M. Boly, M. Massimini, and C. Koch, *Nat. Rev. Neurosci.* **17**, 450 (2016).
- 10) R. Quiñero and S. Panzeri, *Nat. Rev. Neurosci.* **10**, 173 (2009).
- 11) M. Ziegler, C. Wenger, E. Chicca, and H. Kohlstedt, *J. Appl. Phys.* **124**, 152003 (2018).
- 12) D. Seok Jeong, I. Kim, M. Ziegler, and H. Kohlstedt, *RSC Adv.* **3**, 3169 (2013).
- 13) G. W. Burr et al., *Adv. Phys. X* **2**, 89 (2017).
- 14) F. Alibart, E. Zamanidoost, and D. B. Strukov, *Nat. Commun.* **4**, 2072 (2013).
- 15) F. Rosenblatt, *P. Rev.* **65**, 386 (1958).
- 16) Y. Lecun, Y. Bengio, and G. Hinton, *Nature* **521**, 436 (2015).
- 17) G. Indiveri and S. C. Liu, *Proc. IEEE* **103**, 1379 (2015).
- 18) M. Minsky and S. Papert, *Perceptrons Introduction Computational Geometry* (MIT Press, Boston, MA, 1969).
- 19) G. Cybenko, *Math. Control Signals Syst.* **2**, 303 (1989).
- 20) M. Ernout, J. Grollier, and D. Querlioz, *Sci Rep.* **9**, 1851 (2019).
- 21) S. Ambrogio et al., *Nature* **558**, 60 (2018).
- 22) D. B. Strukov, G. S. Snider, D. R. Stewart, and R. S. Williams, *Nat. Lett.* **453**, 80 (2008).
- 23) N. Diederich, T. Bartsch, H. Kohlstedt, and M. Ziegler, *Sci Rep.* **8**, 9367 (2018).
- 24) F. Hadaeghi, X. He, and H. Jaeger, (2017), Unconventional Information Processing Systems, Novel Hardware: A Tour d'Horizon, Technical Report no. 17.
- 25) J. F. Miller, *Nat. Comput.* **18**, 515 (2019).
- 26) A. Z. Stieg, A. V. Avizienis, H. O. Sillin, C. Martin-Olmos, M. Aono, and J. K. Gimzewski, *Adv. Mater.* **24**, 286 (2012).
- 27) M. Di Ventra and F. L. Traversa, *J. Appl. Phys.* **123**, 180901 (2018).
- 28) D. Ielmini and H. S. P. Wong, *Nat. Electron.* **1**, 333 (2018).
- 29) H. O. Sillin, R. Aguilera, H. H. Shieh, A. V. Avizienis, M. Aono, A. Z. Stieg, and J. K. Gimzewski, *Nanotechnology* **24**, 384004 (2013).
- 30) L. Larger, A. Baylón-Fuentes, R. Martinenghi, V. S. Udaltsov, Y. K. Chembo, and M. Jacquot, *Phys. Rev. X* **7**, 1 (2017).
- 31) T. Hasegawa, T. Ohno, K. Terabe, T. Tsuruoka, T. Nakayama, J. K. Gimzewski, and M. Aono, *Adv. Mater.* **22**, 1831 (2010).
- 32) J. M. Parrilla-Gutierrez, A. Sharma, S. Tsuda, G. J. T. Cooper, G. Aragon-Camarasa, K. Donkers, and L. Cronin, *Nat. Commun.* **11**, 1 (2020).
- 33) J. F. Miller, S. L. Harding, and G. Tufte, *Evol. Intell.* **7**, 49 (2014).
- 34) M. Dale, S. Stepney, J. F. Miller, and M. Trefzer, , 2016IEEE Symp. Ser. Comput. Intell. SSCI2016.
- 35) J. B. Mallinson, S. Shirai, S. K. Acharya, S. K. Bose, E. Galli, and S. A. Brown, *Sci. Adv.* **5**, 1 (2019).
- 36) G. Milano, G. Pedretti, M. Fretto, L. Boarino, F. Benfenati, D. Ielmini, I. Valov, and C. Ricciardi, *Adv. Intell. Syst.* **2**, 2000096 (2020).
- 37) K. S. Scharnhorst, J. P. Carbajal, R. C. Aguilera, E. J. Sandouk, M. Aono, A. Z. Stieg, and J. K. Gimzewski, *Jpn. J. Appl. Phys.* **57**, 03ED02 (2018).
- 38) A. Diaz-Alvarez, R. Higuchi, P. Sanz-Leon, I. Marcus, Y. Shingaya, A. Z. Stieg, J. K. Gimzewski, Z. Kuncic, and T. Nakayama, *Sci Rep.* **9**, 14920 (2019).
- 39) S. K. Bose, J. B. Mallinson, R. M. Gazoni, and S. A. Brown, *IEEE Trans. Electron Devices* **64**, 5194 (2017).
- 40) M. Mirigliano, D. Decastri, A. Pullia, D. Dellasega, A. Casu, A. Falqui, and P. Milani, *Nanotechnology* **31**, 234001 (2020).
- 41) M. Mirigliano, S. Radice, A. Falqui, A. Casu, F. Cavaliere, and P. Milani, *Sci Rep.* **10**, 19613 (2020).
- 42) M. Mirigliano, F. Borghi, A. Podestà, A. Antidormi, L. Colombo, and P. Milani, *Nanoscale Adv.* **1**, 3119 (2019).
- 43) M. Mirigliano, B. Paroli, G. Martini, M. Fedrizzi, A. Falqui, A. Casu, and P. Milani, *Neuromorphic Comput. Eng.* **1**, 024007 (2021).
- 44) K. Wegner, P. Piseri, H. V. Tafreshi, and P. Milani, *J. Phys. D: Appl. Phys.* **39**, R439 (2006).
- 45) E. Barborini, P. Piseri, and P. Milani, *J. Phys. D: Appl. Phys.* **32**, L105 (1999).
- 46) P. Piseri, A. Podestà, E. Barborini, and P. Milani, *Rev. Sci. Instrum.* **72**, 2261 (2001).
- 47) M. M. A. Yajadda, K. H. Müller, and K. Ostrikov, *Phys. Rev. B* **84**, 235431 (2011).
- 48) C. Acha, *J. Appl. Phys.* **121**, 134502 (2017).
- 49) T. Burr, A. Seraphin, E. Werwa, and K. Kolenbrander, *Phys. Rev. B* **56**, 4818 (1997).
- 50) W. Chen, H. Ahmed, and K. Nakazoto, *Appl. Phys. Lett.* **66**, 3383 (1995).
- 51) K. H. Muller and M. A. Yajadda, *J. Appl. Phys.* **111**, 123705 (2012).
- 52) S. B. Arnason, S. P. Herschfield, and A. F. Hebard, *Phys. Rev. Lett.* **81**, 3936 (1998).
- 53) W. Steinhögl, G. Schindler, G. Steinlesberger, M. Traving, and M. Engelhardt, *J. Appl. Phys.* **97**, 023706 (2005).
- 54) M. Aguilar, A. I. Oliva, and P. Quintana, *Surf. Sci.* **409**, 501 (1998).
- 55) R. Bo, N. Nasiri, H. Chen, D. Caputo, L. Fu, and A. Tricoli, *ACS Appl. Mater. Interfaces* **9**, 2606 (2017).
- 56) C. Durkan and M. E. Welland, *J. Appl. Phys.* **86**, 1280 (1999).
- 57) M. Mirigliano and P. Milani, *Adv. Phys. X* **6**, 1908847 (2021).
- 58) A. Diaz-Alvarez et al., *AIP Adv.* **10**, 025134 (2020).
- 59) S. Ruder, (2016), An overview of gradient descent optimization algorithms arXiv:1609.04747.
- 60) T. Santaniello, L. Migliorini, Y. Yan, C. Lenardi, and P. Milani, *J. Nanoparticle Res.* **20**, 250 (2018).